Anti-plane fundamental solutions of FGMs and applications to fracture mechanics

J. Li[1], T. Huang[2*], J.H. Yue[3], C. Shi[4], P.H. Wen[4*]

[1]*School of Mathematics and Statistics, Changsha University of Science and Technology, China*

[2]*School o f Communication and Transportation Engineering, Changsha University of Science and Technology, China*

[3]*College of Mathematics, Taiyuan University of Technology, Taiyuan, China*

[4] *School of Engineering and Materials Science, Queen Mary, University of London, London E1 4NS, UK*

Abstract

In this paper, the fundamental solutions for anti-plane elasticity are derived by using the Fourier transform and the Laplace transform techniques, with the shear modulus and the mass density varying exponentially for functionally graded materials. It has been shown that the transformed fundamental solutions both in the Laplace space and in the time domain have the same order of singularities as that in the static case. The time-dependent variables including the displacement and the shear stresses for anti-plane elasticity are obtained with the Durbin's inversion method for the Laplace transform. The Discontinuity Displacement Method is formulated from the fundamental solutions and applied to the mode III fracture problems.

Key words: Fundamental solutions, functionally graded material, anti-plane elasticity, discontinuity displacement method, stress intensity factor.

*Corresponding author: huangtuomao@163.com (T. Huang), p.h.wen@qmul.ac.uk (P.H. Wen)

1. Introduction

In Functionally Graded Materials (FGMs), the variation of the material properties can be pre-determined by controlling the spatial distribution of the composition and the volume fraction of their constituents, which means that the uniform properties are in all directions. These materials have been introduced in recent years to benefit from the ideal performance of its constituents e.g. the high temperature and the corrosion resistance of the ceramics on one side and the large mechanical strength and toughness of the metals on the other by Suresh[1]. For FGMs, we need to solve the differential equations with variable coefficients, because the material properties are dependent on the coordinates. Although the Finite Element Method and Finite Difference Method are well-developed to solve complicated problems, the degree of accuracy needs to be considered. It is well-known that the fundamental solutions for a partial differential equation are essential for numerical analysis in engineering with the Boundary Element Method (BEM), see Brebbia[2], Aliabadi[3,4], Chen & Hong[5], Cheng. & Cheng[6], Clements & Budhi[7]. The spatial variations of the material parameters of FGMs are described by an exponential law for the convenience of analysis. In the family of the BEM, the Method of Fundamental Solution (MFS) is getting more attraction, due to its unique characteristics, see Burgess & Mahajerin[8], Wen[9,10], Fairweather & Karageorghis[11], Golberg & Chen[12], Marin & Lesnic[13]. The main idea of the MFS consists of approximating the solution of the problem by a linear combination of fundamental solutions with some source points located outside the domain, because of the singularity of the fundamental solution. The general problem is transformed to determine the coefficients of the fundamental solutions (known as the density of source), by considering the boundary conditions. In other words, if the source points located outside of the domain are fixed, then the coefficients of the MFS approximation are determined by considering the boundary conditions. To avoid the boundary integration, the MFS has gradually evolved as an effective boundary free method for solving homogeneous partial differential equation (PDE). In addition, if the number of source points tends to infinite and the collocation of source points is on the boundary, the MFS becomes the indirect BEM. Therefore, the MFS retains the same advantage of discretizing only on the boundary but requires no numerical integration. The Discontinuity Displacement Method (DDM) is very similar to the MFS from the super-position principle point of view. However, the DDM can be applied to solve crack problems efficiently, with high degree of accuracy, see Crouch[14], Crouch and

Starfield[15], Dong & Pater[16], Liu[17], Shi et al [18]. The introduction for the DDM under static and dynamic loads both for 2D and 3D problems can be found in a book by Wen[19].

Due to the mathematical complexities for the non-homogeneous nature of FGMs, there are only a few investigations on the transient dynamic responses of cracked FGMs. Jin and Batra[20,21] investigated the interface cracking between the ceramic and/or FGM coatings and a substrate under the anti-plane shear with four coating models by the Boundary Integral Equation Method (BIEM). Reports on their dynamic fracture mechanics are still very few including a numerical treatment of fracture occurring in an FGM under dynamic load by Nakagaki et al [22], the dynamic fracture investigation in FGMs with discrete property variations using dynamic photoelasticity by Parameswaran and Shukla [23], the dynamic fracture mechanics analysis for a composite material with a material inhomogeneity in the thickness direction by Wang et al [24]. Dynamic responses under impact loading have been investigated by Babaei and Lukasiwicz[25]. Li and Zou [26] reported the torsional impact response of an FGM with a penny-shaped crack by using dual integral equations. Li et al [27,28] investigated a functionally graded material with mode III crack under dynamic load using integral equation method. A crack at an arbitrary angle to the graded interfacial zone in bounded media was studied with the shear modulus and the mass density varying in the form of power functions by Choi [29]. The applications of the BEM to FGMs are very limited, as the corresponding time-domain fundamental solutions for general FGMs are either not available or mathematically too complex. Zhang et al [30,31] presented a transient dynamic crack analysis for FGMs by using the BIEM with hyper-singularity in time-domain.

In this paper, the fundamental solutions with point concentrated force and dislocation both in the Laplace domain and the time domain for anti-plane elasticity are derived by using the Fourier and the Laplace transform techniques. These fundamental solutions can be used to obtain the direct/indirect boundary element formulations for static and dynamic anti-plane problems. However, the applications of these fundamental solutions in this paper are demonstrated with the DDM for static and dynamic fracture problems. For FGMs, the boundary integral formulation with dislocation distribution is derived to determine the stress intensity factors. As the fundamental solutions are of hyper-singularity, the Chebyshev polynomial of the second kind is employed. The static and the dynamic stress intensity factors are determined from the coefficients of the Chebyshev polynomials with high accuracy. Comparisons are made with the available exact and the numerical solutions to show the degrees of accuracy and convergence.

2. Fundamental solutions of concentrated force in anti-plane

For the mode III fracture statics with orthotropic FGMs, there are two material coefficients including the shear modulus μ_x and μ_y which are functions of coordinate. It is necessary to make assumptions for these material parameters for mathematical analysis. In static problems, several models have been proposed, such as power function, exponential function and linear function etc (see Li et al [27]). In order to derive the fundamental solution in closed-form, the shear modulus are assumed to vary continuously as $\mu_x = \mu_x^0 e^{2\alpha x+2\beta y}$, $\mu_y = \mu_y^0 e^{2\alpha x+2\beta y}$ in this paper, where μ_x^0 and μ_y^0 are the shear modulus at the origin along the horizontal and vertical directions, α and β are two gradient parameters. Due to the mathematical complexity, it is difficult to obtain the fundamental solution for general material assumptions including dynamic cases.

The equilibrium equation for the anti-plane problem gives

$$\frac{\partial \tau_x}{\partial x} + \frac{\partial \tau_y}{\partial y} = 0, \tag{1}$$

where τ_x and τ_y are the shear stresses. For elasticity, one has

$$\tau_x = \mu_x \frac{\partial w}{\partial x},\ \tau_y = \mu_y \frac{\partial w}{\partial y}\ , \tag{2}$$

where *w* is the anti-plane displacement.

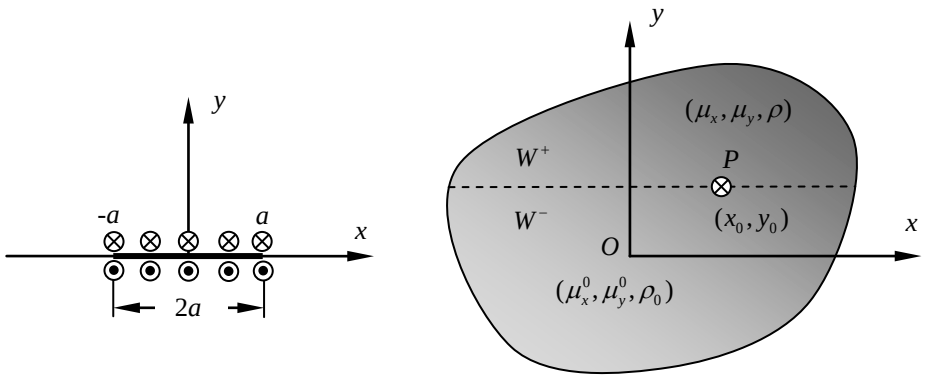

(a) (b)

Figure 1. Infinite FGM sheet with straight crack: (a) crack subjected to anti-plane load on the crack surfaces; (b) anti-plane concentrated force and its location.

Due to the shear modulus varying exponentially in the domain, the equilibrium equation becomes

$$\varepsilon\frac{\partial^2 w}{\partial x^2}+2\alpha\varepsilon\frac{\partial w}{\partial x}+\frac{\partial^2 w}{\partial y^2}+2\beta\frac{\partial w}{\partial y}=0. \tag{3}$$

Applying the Fourier transform

$$w=\frac{1}{2\pi}\int_{-\infty}^{\infty}W(\omega,y)e^{-i\omega x}d\omega, \tag{4}$$

the equilibrium equation (3) yields

$$\frac{d^2W}{dy^2}+2\beta\frac{dW}{dy}-\varepsilon\omega(\omega+2\alpha i)W=0, \tag{5}$$

where $\varepsilon=\mu_x^0/\mu_y^0$ is the orthotropic parameter of FGMs. Therefore, the general solution of displacement are given as

$$W^+=A^+e^{\gamma^+ y} \text{ when } y_0\le y\le\infty \tag{6a}$$

$$W^-=A^-e^{\gamma^- y} \text{ when } -\infty\le y\le y_0 \tag{6b}$$

where A^+ and A^- are coefficients for the upper and lower half-infinite planes respectively, and

$$\gamma^+=-\sqrt{\varepsilon(\omega+\alpha i)^2+\lambda^2}-\beta,\ \gamma^-=\sqrt{\varepsilon(\omega+\alpha i)^2+\lambda^2}-\beta,\ \lambda=\sqrt{\beta^2+\varepsilon\alpha^2}. \tag{7}$$

For a concentrated force Q acting at point $P(x_0,y_0)$, the continuous conditions on the joint line can be described as

$$\tau_y^+-\tau_y^-=Q\delta(x-x_0),\quad w^+-w^-=0,\quad \text{when}\quad y=y_0. \tag{8}$$

Thus, we have two coefficients to be determined:

$$\begin{aligned}&\mu_y^0e^{2\alpha x_0+2\beta y_0}\left[\gamma^+A^+e^{\gamma^+y_0}-\gamma^-A^-e^{\gamma^-y_0}\right]=Qe^{i\omega x_0}\\&A^+e^{\gamma^+y_0}-A^-e^{\gamma^-y_0}=0\end{aligned} \tag{9}$$

The displacement is obtained for the upper half-infinite plane

$$w^+(x,y)=\frac{Qe^{-2\alpha x_0-2\beta y_0}}{\pi\mu_y^0}\int_{-\infty}^{\infty}\frac{e^{\gamma^+(y-y_0)-i\omega(x-x_0)}}{\gamma^+-\gamma^-}d\omega,\ y_0\le y\le+\infty \quad . \tag{10}$$

Consider the integral formula of the Fourier transform

$$\int_{-\infty}^{\infty}\frac{1}{\sqrt{(\omega+\alpha i)^2+\lambda^2}}e^{-y\sqrt{(\omega+\alpha i)^2+\lambda^2}}e^{-i\omega x}d\omega=2e^{-\alpha x}K_0(\lambda\sqrt{x^2+y^2}) \tag{11}$$

Then, from (10), the displacement in the upper half-infinite plane is written as

$$w^+(x,y)=\frac{Q}{2\pi\sqrt{\mu_x^0\mu_y^0}}e^{-\alpha(x+x_0)-\beta(y+y_0)}K_0\left(\lambda\bar{r}\right)\qquad y_0\le y\le+\infty \tag{12}$$

where $\bar{r}=\sqrt{(x-x_0)^2/\varepsilon+(y-y_0)^2}$. It is easy to prove that the fundamental solution (12) is valid for the lower half-infinite plane. Therefore, the displacement fundamental solution under concentrated force *Q* for orthotropic FGMs is

$$w(x,y)=\frac{Q}{2\pi\mu_y^0\sqrt{\varepsilon}}e^{-\alpha(x+x_0)-\beta(y+y_0)}K_0\left(\lambda\bar{r}\right) \tag{13}$$

For the isotropic media, $\varepsilon=1$ and $\mu_x^0=\mu_y^0=\mu_0$, we have

$$w(x,y)=\frac{Q}{2\pi\mu_0}e^{-\alpha(x+x_0)-\beta(y+y_0)}K_0\left(\sqrt{\beta^2+\alpha^2}r\right) \tag{14}$$

where $r=\sqrt{(x-x_0)^2+(y-y_0)^2}$, which is the same, given by Marin & Lesnic[13] for potential problems.

Next, we consider the fundamental solution under dynamic load for orthotropic FGMs. It is assumed that the mass density vary in the same manner as the shear module i.e. $\rho=\rho_0e^{2\alpha x+2\beta y}$, where ρ_0 is the mass density at the origin. Then, the equilibrium equation becomes

$$\varepsilon\frac{\partial^2w}{\partial x^2}+2\alpha\varepsilon\frac{\partial w}{\partial x}+\frac{\partial^2w}{\partial y^2}+2\beta\frac{\partial w}{\partial y}=\frac{\rho_0}{\mu_y^0}\frac{\partial^2w}{\partial t^2} \tag{15}$$

Applying the Fourier and the Laplace transforms over the equilibrium equation, with zero initial conditions gives

$$-\varepsilon\omega(\omega+2\alpha i)\tilde{W}+\frac{d^2\tilde{W}}{dy^2}+2\beta\frac{d\tilde{W}}{dy}-\frac{p^2}{c^2}\tilde{W}=0 \tag{16}$$

in which $c=\sqrt{\mu_y^0/\rho_0}$ is the velocity of the shear elastic wave along the y axis and

$$\tilde{W}(\omega,y,p)=\int_0^\infty W(\omega,y,t)e^{-pt}dt \tag{17}$$

Then, the roots of the characteristic equation (16) are

$$\tilde{\gamma}^+=-\sqrt{\varepsilon(\omega+\alpha i)^2+\overline{\lambda}}-\beta,\ \tilde{\gamma}^-=\sqrt{\varepsilon(\omega+\alpha i)^2+\overline{\lambda}}-\beta,\ \overline{\lambda}=\sqrt{\lambda^2+p^2/c^2}. \tag{18}$$

The general solutions of displacement of (16) are

$$\tilde{W}^+=\tilde{A}^+e^{\tilde{\gamma}^+y}\ \text{when}\ y_0\le y\le\infty \tag{19a}$$

$$\widetilde{W}^{-} = \widetilde{A}^{-} e^{\widetilde{\gamma}^{-} y} \text{ when } -\infty \le y \le y_0 \tag{19b}$$

where $\widetilde{A}^{+}$ and $\widetilde{A}^{-}$ are the coefficients. The continuous conditions with a concentrated shear force Q, acting at point P, in time domain give

$$\tau_y^{+} - \tau_y^{-} = Q\delta(x - x_0)\delta(t), \quad w^{+} - w^{-} = 0, \qquad y = y_0 \tag{20}$$

Thus, two coefficients can be obtained from

$$\begin{aligned} &\mu_y^0 e^{2\alpha x_0 + 2\beta y_0}\left[\widetilde{\gamma}^{+}\widetilde{A}^{+} e^{\widetilde{\gamma}^{+} y_0} - \widetilde{\gamma}^{-}\widetilde{A}^{-} e^{\widetilde{\gamma}^{-} y_0}\right] = Q e^{i\omega x_0} \\ &\widetilde{A}^{+} e^{\widetilde{\gamma}^{+} y_0} - \widetilde{A}^{-} e^{\widetilde{\gamma}^{-} y_0} = 0 \end{aligned} \tag{21}$$

As for static case, the displacement fundamental solution in the Laplace transform domain under concentrated force $Q\delta(t)$ for orthotropic FGMs is obtained

$$\widetilde{W}(x, y, p) = \frac{Q}{2\pi\mu_y^0\sqrt{\varepsilon}} e^{-\alpha(x+x_0)-\beta(y+y_0)} K_0\left(\overline{\lambda}\overline{r}\right) \tag{22}$$

with the shear stresses

$$\begin{aligned} \widetilde{\tau}_x(x - x_0, y - y_0, p) &= -\frac{Q}{2\pi}\sqrt{\varepsilon} e^{\alpha(x-x_0)+\beta(y-y_0)}\left[\alpha K_0(\overline{\lambda}\overline{r}) + \overline{\lambda} K_1(\overline{\lambda}\overline{r})\frac{x - x_0}{\varepsilon\,\overline{r}}\right] \\ \widetilde{\tau}_y(x - x_0, y - y_0, p) &= -\frac{Q}{2\pi\sqrt{\varepsilon}} e^{\alpha(x-x_0)+\beta(y-y_0)}\left[\beta K_0(\overline{\lambda}\overline{r}) + \overline{\lambda} K_1(\overline{\lambda}\overline{r})\frac{y - y_0}{\overline{r}}\right] \end{aligned} \tag{23}$$

Again, for the isotropic media, the fundamental solution of displacement is given, in the Laplace domain as

$$\widetilde{W}(x, y, p) = \frac{Q}{2\pi\mu_0} e^{-\alpha(x+x_0)-\beta(y+y_0)} K_0\left(\overline{\lambda} r\right). \tag{24}$$

Consider the inversion of the Laplace transform by Bateman[32], the fundamental solution of displacement in the time domain is given by

$$W(x, y, t) = \frac{Q}{2\pi\mu_y^0\sqrt{\varepsilon}} e^{-\alpha(x+x_0)-\beta(y+y_0)} F(c, \lambda, \overline{r}, t) \tag{25}$$

where

$$F(c, \lambda, \overline{r}, t) = \frac{c}{\overline{r}}\left[f(ct/\overline{r}) - c\lambda\int_0^t f(c\sqrt{t^2 - u^2}/\overline{r}) J_1(c\lambda u) du \right] \tag{26}$$

in which

$$f(t)=\begin{cases}0 & 0<t<1\\ \dfrac{1}{\sqrt{t^2-1}} & t>1\end{cases} \tag{27}$$

where $J_1(z)$ is the Bessel function. Substituting (27) into (26) gives,

$$F(c,\lambda,\bar{r},t)=\begin{cases}0 & 0<t<\bar{r}/c\\ \dfrac{1}{\sqrt{t^2-\bar{r}^2/c^2}}-c\lambda\displaystyle\int_0^{\sqrt{t^2-\bar{r}^2/c^2}}\frac{J_1(c\lambda u)du}{\sqrt{t^2-\bar{r}^2/c^2-u^2}} & t>/\bar{r}/c\end{cases} \tag{28}$$

It is clear that the time-dependent displacement is zero before the arrival of the elastic shear wave. The shear stresses can be obtained:

$$\begin{aligned}\tau_x(x-x_0,y-y_0,t)&=\frac{Q}{2\pi}\sqrt{\varepsilon}e^{\alpha(x-x_0)+\beta(y-y_0)}\left[-\alpha F(c,\lambda,\bar{r},t)+\frac{\partial F}{\partial\bar{r}}\frac{x-x_0}{\varepsilon\,\bar{r}}\right]\\ \tau_y(x-x_0,y-y_0,t)&=\frac{Q}{2\pi\sqrt{\varepsilon}}e^{\alpha(x-x_0)+\beta(y-y_0)}\left[-\beta F(c,\lambda,\bar{r},t)+\frac{\partial F}{\partial\bar{r}}\frac{y-y_0}{\bar{r}}\right]\end{aligned} \tag{29}$$

Consider a concentrated force with the Heaviside function i.e. $QH(t)$, the fundamental solution of displacement in the Laplace domain is

$$\tilde{W}_H(x,y,p)=\frac{Q}{2p\pi\sqrt{\mu_x^0\mu_y^0}}e^{-\alpha(x+x_0)-\beta(y+y_0)}K_0\left(\bar{\lambda}\bar{r}\right) \tag{30}$$

and the shear stresses are

$$\begin{aligned}\tilde{\tau}_x^H(x-x_0,y-y_0,p)&=-\frac{Q}{2p\pi}\sqrt{\varepsilon}e^{\alpha(x-x_0)+\beta(y-y_0)}\left[\alpha K_0(\bar{\lambda}\bar{r})+\bar{\lambda}K_1(\bar{\lambda}\bar{r})\frac{x-x_0}{\varepsilon\,\bar{r}}\right]\\ \tilde{\tau}_y^H(x-x_0,y-y_0,p)&=-\frac{Q}{2p\pi\sqrt{\varepsilon}}e^{\alpha(x-x_0)+\beta(y-y_0)}\left[\beta K_0(\bar{\lambda}\bar{r})+\bar{\lambda}K_1(\bar{\lambda}\bar{r})\frac{y-y_0}{\bar{r}}\right]\end{aligned} \tag{31}$$

By using the formula of the Laplace transform inverse, the fundamental solutions in the time domain can be obtained

$$W_H(x,y,t)=\frac{Q}{2\pi\sqrt{\mu_x^0\mu_y^0}}e^{-\alpha(x+x_0)-\beta(y+y_0)}F_{\mathrm{H}}(c,\lambda,\bar{r},t) \tag{32}$$

where

$$\begin{aligned}F_{\mathrm{H}}(c,\lambda,\bar{r},t)&=\int_0^t F(c,\lambda,\bar{r},t)dt\\ &=\begin{cases}0 & 0<t<\bar{r}/c\\ \displaystyle\int_{\bar{r}/c}^t\frac{dt}{\sqrt{t^2-\bar{r}^2/c^2}}-c\lambda\int_{\bar{r}/c}^t\int_0^{\sqrt{t^2-\bar{r}^2/c^2}}\frac{J_1(c\lambda u)dudt}{\sqrt{t^2-u^2-\bar{r}^2/c^2}} & t>/\bar{r}/c\end{cases}\end{aligned} \tag{33}$$

The integral domain is shown in Figure 2. By changing the order of the integration, we have

$$\int_{\bar{r}/c}^{t}\int_{0}^{\sqrt{t^2-\bar{r}^2/c^2}}\frac{J_1(c\lambda u)dudt}{\sqrt{t^2-u^2-\bar{r}^2/c^2}}=\int_{0}^{\sqrt{t^2-\bar{r}^2/c^2}}J_1(c\lambda u)du\int_{\sqrt{u^2+\bar{r}^2/c^2}}^{t}\frac{dt}{\sqrt{t^2-u^2-\bar{r}^2/c^2}}$$
$$=\int_{0}^{\sqrt{t^2-\bar{r}^2/c^2}}J_1(c\lambda u)\times\ln\frac{t+\sqrt{t^2-u^2-\bar{r}^2/c^2}}{\sqrt{u^2+\bar{r}^2/c^2}}du \tag{34}$$

Therefore, (33) can be written as

$$F_{\mathrm{H}}(c,\lambda,\bar{r},t)=\begin{cases}0 & 0<t<\bar{r}/c\\ \ln\dfrac{t+\sqrt{t^2-\bar{r}^2/c^2}}{\bar{r}/c}-c\lambda\displaystyle\int_{0}^{\sqrt{t^2-\bar{r}^2/c^2}}J_1(c\lambda u)\times\ln\frac{t+\sqrt{t^2-u^2-\bar{r}^2/c^2}}{\sqrt{u^2+\bar{r}^2/c^2}}du & t>/\bar{r}/c\end{cases} \tag{35}$$

Therefore the shear stresses can be obtained

$$\tau_x^H(x-x_0,y-y_0,t)=\frac{Q}{2\pi}\sqrt{\varepsilon}e^{\alpha(x-x_0)+\beta(y-y_0)}\left[-\alpha F_{\mathrm{H}}(c,\lambda,\bar{r},t)+\frac{\partial F_{\mathrm{H}}}{\partial\bar{r}}\frac{x-x_0}{\varepsilon\,\bar{r}}\right]$$
$$\tau_y^H(x-x_0,y-y_0,t)=\frac{Q}{2\pi\sqrt{\varepsilon}}e^{\alpha(x-x_0)+\beta(y-y_0)}\left[-\beta F_{\mathrm{H}}(c,\lambda,\bar{r},t)+\frac{\partial F_{\mathrm{H}}}{\partial\bar{r}}\frac{y-y_0}{\bar{r}}\right] \tag{36}$$

in which

$$\frac{\partial F_{\mathrm{H}}}{\partial\bar{r}}=\frac{1}{\bar{r}}\begin{cases}0 & 0<\bar{t}<1\\ -A(\bar{t})-\bar{r}\lambda\displaystyle\int_{0}^{\sqrt{\bar{t}^2-1}}J_1(\bar{r}\lambda u)B(\bar{t},u)du & \bar{t}>1\end{cases} \tag{37}$$

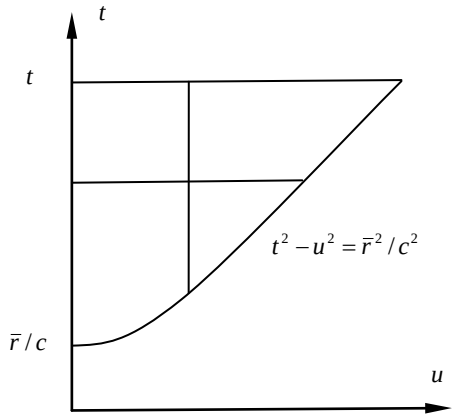

Figure 2. Integration domain and changing the integral order.

where $\bar{t} = ct/\bar{r}$ and the dimensionless functions $A(\bar{t})$ and $B(\bar{t},u)$ are defined as

$$A(\bar{t}) = \frac{1}{\left(\bar{t}+\sqrt{\bar{t}^2-1}\right)\sqrt{\bar{t}^2-1}}+1,$$
$$B(\bar{t},u) = \frac{1}{\left(\bar{t}+\sqrt{\bar{t}^2-(1+u^2)}\right)\sqrt{\bar{t}^2-(1+u^2)}}+\frac{1}{1+u^2}. \tag{38}$$

Finally, we consider the fundamental solution for a dislocation, as shown in Figure 3. Consider two reference cases. The first case is a dislocation located at the coordinate $T(x_0, y_0)$ along the local axis x' with a slant angle θ against axis *x*. The second case is a unit concentrated shear force $(Q=1)$ acting at the point $P(x,y)$. Applying the principal of reciprocity over these two reference cases, we have the fundamental solution of displacement with a dislocation as

$$\tilde{W}_D(x,y,p) = \tilde{\tau}_x(x_0-x, y_0-y, p)\sin\theta - \tilde{\tau}_y(x_0-x, y_0-y, p)\cos\theta \tag{39}$$

in which $\tilde{\tau}_x(x_0-x, y_0-y, p)$ and $\tilde{\tau}_y(x_0-x, y_0-y, p)$ are the fundamental solutions of the shear stress shown in (23). Therefore, the fundamental solution of displacement with a dislocation is written, in the Laplace domain as

$$\tilde{W}_D(x,y,p) = -\frac{1}{2\pi}e^{-\alpha(x-x_0)-\beta(y-y_0)}\left[\left(\sqrt{\varepsilon}\alpha\sin\theta-\frac{\beta\cos\theta}{\sqrt{\varepsilon}}\right)K_0(\bar{\lambda}\bar{r})-\right.$$
$$\left.\frac{\bar{\lambda}K_1(\bar{\lambda}\bar{r})}{\sqrt{\varepsilon}\bar{r}}\left[(x-x_0)\sin\theta-(y-y_0)\cos\theta\right]\right]. \tag{40}$$

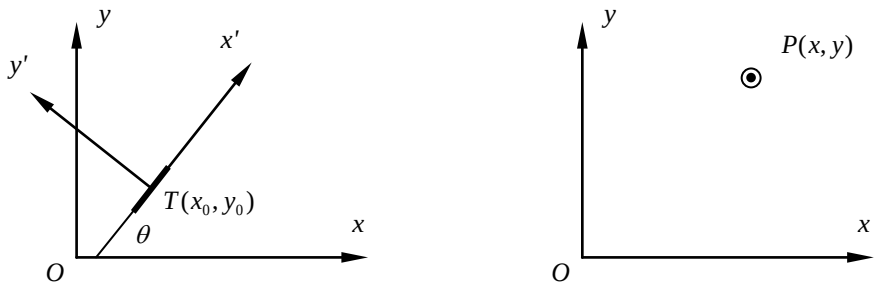

(a) (b)

Figure 3. Two load cases: (a) Dislocation with angle θ; (b) Concentrated anti-plane force。

By Hooke's law, we can easily obtain the fundamental solutions of the shear stresses from (40). It is worth pointing out that the constant element is the most popular approach for the Displacement Discontinuity Method (DDM) in engineering by Crouch & Starfield[15] and Wen[19].

To demonstrate the effect due to the gradient coefficients of functionally graded materials, the time responses of the shear stress is observed. Consider a unit concentrated shear force acting at the origin, $Q(t) = P_0 H(t)$, $\alpha = 0$ and β is chosen as 0, 0.5 and 1 respectively. The normalized shear stress $\tau_y a / P_0$ versus the normalized time at the observing point (a, a) is shown in Figures 4(a), 4(b) and 4(c) with different material properties. The effect by the gradient parameter β is shown in Figure 4(a) when constants $\alpha = 0, \varepsilon = 1$. The effect by parameter α is also presented in Figure 4(b) in the case of $\beta = 0, \varepsilon = 1$. In Figure 4(c), the response of stress is shown when $\alpha = \beta = 1$ for different ratio of ε. Obviously the stress is kept at zero until the shear elasticity wave arrived travelling from the load acting point. There is no oscillation for isotropic homogenous material ($\alpha = \beta = 0$) at the observing point from Figures 4(a) and 4(b). However, the oscillations are seen for functionally graded materials in these figures. Obviously the oscillation caused by the gradient of materials is significant. In addition, the frequency of the oscillation increases when the gradient parameters α and β increase.

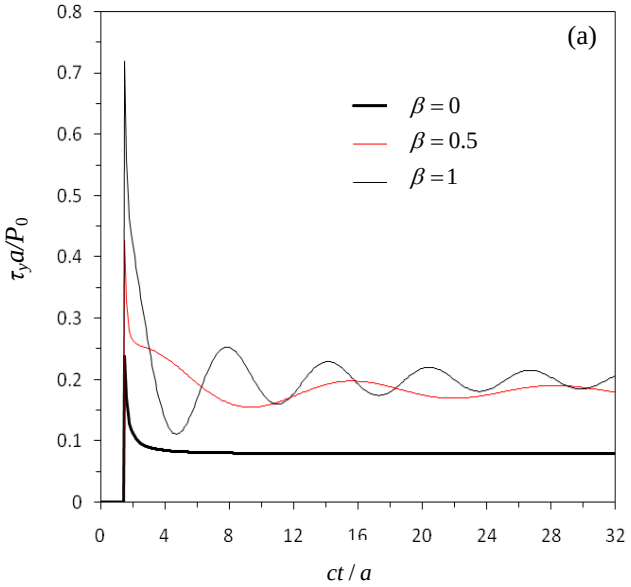

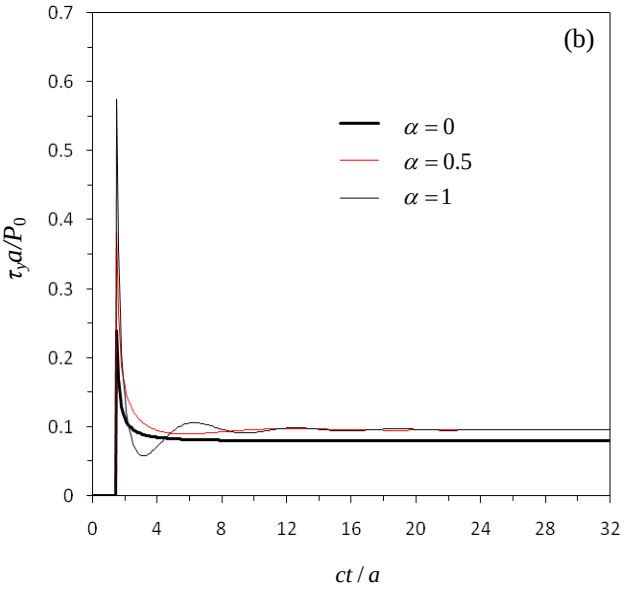

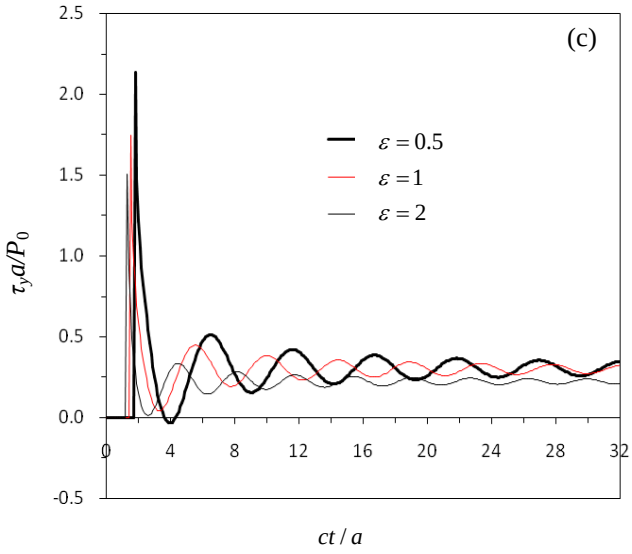

Figure 4. Effects of the FGM constants. (a) $\alpha = 0, \varepsilon = 1$ and β is variable; (b) $\beta = 0, \varepsilon = 1$ and α is variable; (c) $\alpha = \beta = 1$ and ε is variable.

3. Integral equation of displace discontinuity for a crack

For the sake of simplicity, we consider a straight crack on the axis *x*, as shown in Figure 1(a). The fundamental solution for a dislocation at the origin in the Laplace space is obtained from (40) by letting $\theta = 0$.

$$\widetilde{W}_D(x,y,p)=\frac{1}{2\pi\sqrt{\varepsilon}}e^{-\alpha(x-x_0)-\beta(y-y_0)}\left[\beta K_0(\overline{\lambda}\overline{r})-\overline{\lambda}K_1(\overline{\lambda}\overline{r})\frac{y-y_0}{\overline{r}}\right] \tag{41}$$

Thus the shear stress is obtained

$$\widetilde{\tau}_y^D(x,x_0,y,y_0,p)=\frac{\mu_y^0 e^{\alpha(x+x_0)+\beta(y+y_0)}}{2\pi\sqrt{\varepsilon}}\left[\left(\frac{\overline{\lambda}^2(y-y_0)^2}{\overline{r}^2}-\beta^2\right)K_0(\overline{\lambda}\overline{r})+\frac{\overline{\lambda}[(y-y_0)^2-(x-x_0)^2]}{\overline{r}^3}K_1(\overline{\lambda}\overline{r})\right] \tag{42}$$

Therefore, the shear stress along the axis x, by letting $x_0=\xi$ and $y=y_0=0$ in (42) above becomes

$$\widetilde{\tau}_y^D(x,\xi,0,0,p)=\widetilde{Y}(x,\xi,p)=\frac{-\mu_y^0}{2\pi\sqrt{\varepsilon}}e^{\alpha(x+\xi)}\left[\beta^2K_0(\overline{\lambda}(x-\xi)/\sqrt{\varepsilon})+\frac{\overline{\lambda}}{x-\xi}K_1(\overline{\lambda}(x-\xi)/\sqrt{\varepsilon})\right] \tag{43}$$

Obviously the hyper-singular term in the shear stress above is

$$T(x,\xi)=-\frac{\mu_y^0 e^{\alpha(x+\xi)}}{2\pi(x-\xi)^2}. \tag{44}$$

which is independent of the orthotropic parameter ε. Consider a straight crack of length 2a with the density of the discontinuity displacement $\widetilde{\psi}(x)(=\Delta\widetilde{W}=[\widetilde{W}^+-\widetilde{W}^-])$ on its surface in the region $-a\le x\le a$, as shown in Figure 1(a). The boundary integral equation can be written as

$$\int_{-a}^{a}\widetilde{Y}(x,\xi,p)\widetilde{\psi}(\xi)d\xi=-\widetilde{\tau}_0(x,p),\qquad -a\le x\le a \tag{45}$$

where $\widetilde{\tau}_0(x,p)$ is the applied anti-plane shear force. Taking the second degree of the Hadamard's finite part in Eq. (45) yields

$$\begin{aligned}&\int_{-a}^{a}\frac{\widetilde{\psi}(\xi)e^{\alpha(x+\xi)}}{|x-\xi|^2}d\xi+\int_{-a}^{a}E(x,\xi,p)\widetilde{\psi}(\xi)d\xi=\frac{2\pi\widetilde{\tau}_0(x,p)}{\mu_y^0},\qquad -a\le x\le a\\ &E(x,\xi,p)=\frac{1}{\sqrt{\varepsilon}}e^{\alpha(x+\xi)}\left[\beta^2K_0(\overline{\lambda}(x-\xi)/\sqrt{\varepsilon})+\frac{\overline{\lambda}}{x-\xi}K_1(\overline{\lambda}(x-\xi)/\sqrt{\varepsilon})-\frac{1}{(x-\xi)^2}\right]\end{aligned} \tag{46}$$

in which the function $E(x)$ is of weak singular $O(\ln r)$. Because of the shear stress being of singularity $O(r^{-1/2})$ at the crack tips $x=\pm a$, we assume that

$$\widetilde{\psi}(x,p)=\sqrt{a^2-x^2}e^{-\alpha x}\sum_{k=0}^{K}c_kU_k(x/a), \tag{47}$$

where c_k represents the coefficient, $U_k(x/a)$ are the Chebyshev polynomials of the second kind i.e.

$$U_k(x/a)=\frac{\sin[(k+1)\arccos(x/a)]}{\sin[\arccos(x/a)]}. \tag{48}$$

Due to the integral formula given by Kaya and Erdogan[33],

$$\int_{-a}^{a}\frac{\sqrt{a^2-\xi^2}U_k(\xi/a)}{(x_i-\xi)^2}d\xi=-\pi(k+1)U_k(x_i/a), \tag{49}$$

where the collocation points x_i are chosen as

$$x_k/a=\cos\left(\frac{(2i+1)}{2(K+1)}\pi\right),\ i=0,1,2,...,K, \tag{50}$$

Then, Eq.(46) at the collocation point x_i becomes

$$\sum_{k=0}^{K}c_k e^{\alpha x}\left[-\pi(k+1)U_k(x_i/a)+\int_{-a}^{a}E(x_i,\xi,p)\sqrt{a^2-\xi^2}U_k(\xi/a)d\xi\right]=\frac{2\pi\tilde{\tau}_0(x_i,p)}{\mu_y^0},\ i=0,1,...,K. \tag{51}$$

In order to cancel the weak singularity in $E(x_i,\xi)$, a coordinate transformation is introduced i.e. $\xi'=\sqrt{\xi-x_i}$. Eq.(51) provides a set of linear system of equations with K + 1 unknowns c_k to be determined. As the displacement field at the crack tips for FGMs is the same as isotropic materials near the crack tip i.e.

$$\begin{aligned}\tilde{\psi}(\pm a,p)&=\lim_{r\to 0}\frac{2\tilde{K}_{III}(\pm a)}{\pi\mu_y(\pm a)}\sqrt{2\pi r}\\ \tilde{K}_{III}(\pm a)&=\frac{\sqrt{\pi}\mu_y(\pm a)}{2}\lim_{r\to 0}\frac{\tilde{\psi}(\pm a,p)}{\sqrt{2r}}\end{aligned} \tag{52}$$

where $\tilde{K}_{III}$ indicates the stress intensity factor. Therefore, the stress intensity factors can be determined directly by the displacement discontinuity, from Eq.(47), as

$$\tilde{K}_{III}(\pm a,p)=\frac{\mu_y^0 e^{\pm\alpha a}}{2}\sum_{k=0}^{K}c_k U_k(\pm 1)\sqrt{\pi a}, \tag{53}$$

From the properties of the Chebyshev polynomials, $U_k(+1)=k+1$ and $U_k(-1)=(-1)^k(k+1)$. In the following numerical examples, the number K in Eq.(50) is taken to 15 in this example.

By selecting $(L+1)$ samples in the Laplace space $p_l, l=0,1,...,L$, $\tilde{K}_{III}(\pm a,p_l)$ is evaluated for each Laplace parameter from Eq.(53). Thereafter, the time-dependent function $\tilde{K}_{III}$ in the time domain can be determined by the Laplace inversion techniques. By selecting

$p_l = (\sigma + 2l\pi i)/T \quad (i = \sqrt{-1})$, an accurate inverse method proposed by Durbin[34] is adopted here, as follows

$$\tilde{K}_{III}(t) = \frac{2e^{\sigma t/T}}{T}\left[-\frac{1}{2}\tilde{K}_{III}(p_0) + \sum_{l=0}^{L} \mathrm{Re}\left\{\tilde{K}_{III}(p_l)e^{2l\pi i t/T}\right\}\right] \tag{54}$$

In the Durbin's inverse formula in Eq.(54), there are two free parameters σ and T. In fact, the parameter T depends on the observing period of time and σ is taken to 5 in all examples below.

4. Numerical examples and discussion

Example 4.1 Functionally graded media under static load on crack surface

First we consider a straight crack between $(-a, a)$ subjected to a uniform shear load τ_0 on the crack surfaces. In the static analysis of the functionally graded materials, there are two material parameters including two gradient parameters α and β when the orthotropic parameter $\varepsilon = 1$. Numerical results of the normalized stress intensity factor $K_{III}^{(\pm)}/\tau_0\sqrt{\pi a}$ are shown in Table 1 and Table 2 for different material parameters, i.e. the gradient parameters α and β are selected as 0, 0.25, 0.5, 0.75 and 1 respectively. The same problems were studied by Li et al [27] analytically and by Zhang et al.[31] using the Boundary Integral Equation Method (BIEM) which can be used to examine the degree of accuracy in this paper. It shows that the difference between the BIEM and the DDM is very small (see the numerical results for static case listed in Table 1 and Table 2 by Zhang el at.[31]) and they are identical when $\alpha = 0$, as shown in these tables.

Second, we consider a slant crack in FGMs, as shown in Figure 5 with $\alpha' = 0, \varepsilon' = 1$ and β' is free variable in the coordinate $(x'oy')$. Therefore, in the new coordinate system (x, y), one has

$$\mu_x = \mu_y = \mu_y^0 e^{2\beta(x\sin\theta + y\cos\theta)} \tag{55}$$

So we have two gradient parameters in the new system (xoy)

$$\alpha = \beta'\sin\theta, \quad \beta = \beta'\cos\theta, \quad \varepsilon = 1. \tag{56}$$

The normalized stress intensity factors are presented in Table 3 for different gradient parameters β' and crack orientations θ.

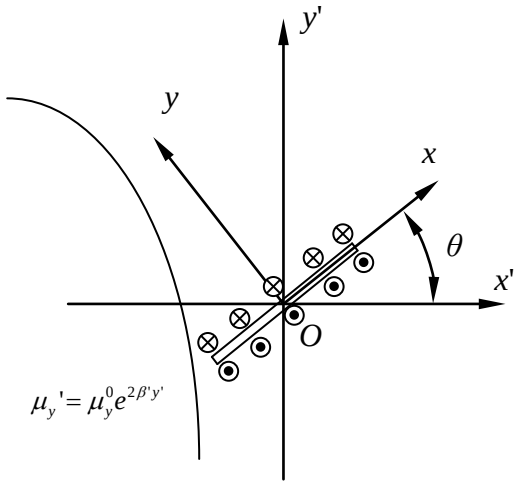

Figure 5. A slant crack with orientation θ in two coordinates.

Table 1. Stress intensity factors $K_{III}(a)/\tau_0\sqrt{\pi a}$ while $\varepsilon = 1$.

α\β	0.00	0.25	0.50	0.75	1.00	1.25	1.50	1.75	2.00	2.25	2.50
0.00	1.0000	1.0280	1.0762	1.1308	1.1875	1.2444	1.3007	1.3559	1.4099	1.4625	1.5137
0.25	1.0906	1.1234	1.1865	1.2565	1.3277	1.3983	1.4675	1.5348	1.6002	1.6637	1.7253
0.50	1.1438	1.1722	1.2396	1.3219	1.4078	1.4931	1.5764	1.6570	1.7350	1.8103	1.8830
0.75	1.1765	1.2002	1.2625	1.3465	1.4395	1.5348	1.6291	1.7211	1.8102	1.8963	1.9793
1.00	1.1974	1.2174	1.2725	1.3518	1.4445	1.5432	1.6433	1.7424	1.8394	1.9336	2.0248
1.25	1.2114	1.2286	1.2770	1.3495	1.4378	1.5350	1.6363	1.7384	1.8396	1.9388	2.0354
1.50	1.2213	1.2362	1.2790	1.3447	1.4271	1.5202	1.6195	1.7214	1.8239	1.9254	2.0251
1.75	1.2285	1.2417	1.2798	1.3394	1.4156	1.5036	1.5992	1.6990	1.8006	1.9024	2.0033
2.00	1.2340	1.2457	1.2801	1.3343	1.4047	1.4873	1.5784	1.6750	1.7745	1.8752	1.9757
2.25	1.2382	1.2488	1.2800	1.3296	1.3947	1.4722	1.5587	1.6514	1.7479	1.8466	1.9460
2.50	1.2416	1.2513	1.2797	1.3254	1.3859	1.4584	1.5403	1.6290	1.7223	1.8184	1.9158

Table 2. Stress intensity factors $K_{III}(-a)/\tau_0\sqrt{\pi a}$ while $\varepsilon = 1$.

α\β	0.00	0.25	0.50	0.75	1.00	1.25	1.50	1.75	2.00	2.25	2.50
0.00	1.0000	1.0280	1.0762	1.1308	1.1875	1.2444	1.3007	1.3559	1.4099	1.4625	1.5137
0.25	0.8570	0.8775	0.9178	0.9631	1.0099	1.0568	1.1031	1.1486	1.1930	1.2363	1.2786
0.50	0.7291	0.7406	0.7683	0.8030	0.8401	0.8777	0.9151	0.9519	0.9880	1.0232	1.0576
0.75	0.6309	0.6373	0.6544	0.6780	0.7050	0.7333	0.7622	0.7910	0.8194	0.8474	0.8748
1.00	0.5576	0.5614	0.5719	0.5874	0.6061	0.6266	0.6480	0.6698	0.6917	0.7135	0.7350
1.25	0.5025	0.5048	0.5115	0.5218	0.5347	0.5493	0.5650	0.5814	0.5981	0.6149	0.6318
1.50	0.4599	0.4615	0.4660	0.4730	0.4820	0.4926	0.5042	0.5165	0.5293	0.5424	0.5556
1.75	0.4262	0.4273	0.4304	0.4354	0.4419	0.4497	0.4584	0.4678	0.4778	0.4880	0.4985
2.00	0.3989	0.3996	0.4019	0.4056	0.4104	0.4163	0.4229	0.4303	0.4380	0.4462	0.4546
2.25	0.3761	0.3767	0.3784	0.3811	0.3849	0.3894	0.3946	0.4004	0.4066	0.4131	0.4200
2.50	0.3568	0.3573	0.3586	0.3607	0.3636	0.3672	0.3713	0.3760	0.3810	0.3864	0.3920

Table 3. Stress intensity factors $K_{III}^{(\pm)} / \tau_0 \sqrt{\pi a}$ for isotropic FGMs while $\alpha' = 0$.

β'\θ	$K_{III}^{+} / \tau_0 \sqrt{\pi a}$					$K_{III}^{-} / \tau_0 \sqrt{\pi a}$				
	0^0	30^0	45^0	60	90^0	0^0	30^0	45^0	60	90^0
0.00	1.0000	1.0000	1.0000	1.0000	1.0000	1.0000	1.0000	1.0000	1.0000	1.0000
0.25	1.0280	1.0777	1.0878	1.0910	1.0906	1.0280	0.9500	0.9125	0.8826	0.8570
0.50	1.0762	1.1685	1.1726	1.1618	1.1438	1.0762	0.9062	0.8302	0.7740	0.7291
0.75	1.1308	1.2643	1.2530	1.2195	1.1765	1.1308	0.8629	0.7563	0.6843	0.6309
1.00	1.1875	1.3616	1.3288	1.2682	1.1974	1.1875	0.8200	0.6921	0.6128	0.5576
1.25	1.2444	1.4584	1.4000	1.3106	1.2114	1.2444	0.7785	0.6374	0.5562	0.5025
1.50	1.3007	1.5534	1.4671	1.3487	1.2213	1.3007	0.7390	0.5910	0.5111	0.4599
1.75	1.3559	1.6459	1.5306	1.3837	1.2285	1.3559	0.7022	0.5518	0.4746	0.4262
2.00	1.4099	1.7354	1.5911	1.4164	1.2340	1.4099	0.6683	0.5185	0.4445	0.3989
2.25	1.4625	1.8219	1.6489	1.4475	1.2382	1.4625	0.6373	0.4901	0.4193	0.3761
2.50	1.5137	1.9053	1.7045	1.4772	1.2416	1.5137	0.6092	0.4655	0.3979	0.3568

Example 4.2 Functionally graded media under dynamic load on crack surface

Consider the same crack of length 2*a* in FGMs, subjected to dynamic shear force $\tau_0 H(t)$ in time domain and τ_0 / p in the Laplace domain. The number of samples in the Laplace space is chosen as $L = 200$ with two free parameters $\sigma = 5, T = 20$ in the Durbin's inversion method. Several FGMs are considered as follows

Case 1: Gradient parameter $\theta = \beta = 0, \varepsilon = 1$ and α varies from 0 to 1;

Case 2: Gradient parameter $\theta = \alpha = 0, \varepsilon = 1$ and β varies from 0 to 1;

Case 3: Gradient parameter $\alpha = 0, \beta = 0.5, \varepsilon = 1$ and crack orientation θ is variable;

Case 4: Orthotropic parameter ε varies from 0.25 to 4 when $\alpha = 1, \beta = \theta = 0$.

The normalized stress intensity factors $K_{III}(t) / \tau_0 \sqrt{\pi a}$ for each case are presented from Figure 6 to Figure 9 versus dimensionless time ct / a. These results show that the gradient parameters have significant influences on the transient dynamic stress intensity factors, particularly at the tip of the right-hand-side. In Case 1, the normalized dynamic stress intensity factors at the right crack-tip are larger than that at left crack-tip, when the gradient parameter α is large than zero. In other words, the normalized dynamic stress intensity factors at the right crack-tip $K_{III}^{(+)}$ increase when the gradient parameter α increases. However, the normalized factors at the left crack-tip $K_{III}^{(-)}$ decrease when α increases. Because the shear modulus at the right crack-tip is always larger than that at the left crack-tip when the gradient parameter $\alpha > 0$, it is shown that the stress intensity factor is bigger as expected. Similar to the shear stress response for a concentrated shear force

shown in Figure 4, the oscillation for the dynamic stress intensity factor at the right crack-tip is obvious when the parameter α is larger. However, the oscillation is relatively weaker at the left crack-tip, as shown in Figures 6(a) and 6(b). In Case 2, the stress intensity factors are the same at two crack tips, due to symmetry. It can be observed that the oscillation is huge when β is taken to 1, as shown in Figure 7. Again, the normalized dynamic stress intensity factor at the right crack-tip K_{III} increases when the gradient parameter β increases. However, the oscillation of the curve K_{III} versus the normalized time caused by the gradient parameter is significant when $\beta > 0.75$. In Case 3, the results are similar to Case 1 and the influence caused by the orientation of the crack is significant from Figures 8(a) and 8(b). In Case 4, the effect of the orthotropic parameter ε can be seen clearly from Figures 9(a) and 9(b). Since the arrival times of the shear elasticity wave travelling from the left crack-tip to the right crack-tip are different for different orthotropic parameters, the corresponding times for the picks are also different. However, the maximum values of the dynamic stress intensity factors at each crack-tip are almost the same. In addition, for each case, the picks are collocated at time $ct/a = 2\sqrt{\varepsilon}$, as expected. From these numerical examples, it can be concluded as following

(1) The gradient parameters of material α, β and the ratio ε may have significant influence on the stress intensity factor and causes oscillations. The peak value of the normalized stress intensity factors increases with increasing gradient parameters α and β;

(2) The stress intensity factor at the crack tip with the bigger shear modulus (right crack-tip) is larger than that with smaller modulus (left crack-tip), i.e. $K_{III}^{(+)} > K_{III}^{(-)}$;

(3) For isotropic FGMs under both static and dynamic load, the degree of accuracy is observed with semi-analytical solutions given by Zhang et al [31] and analytical solution by Li et al [27]. It is shown that the difference is very small compared with different approaches.

Finally, it is worth to mention that the FGMs are innovative composite materials whose composition and microstructure vary in space following a predetermined law[35,36]. The gradual change in composition and microstructure gives place to a gradient of properties and performances. The investigation in this paper concentrated on the evaluation of stress intensity factors under dynamic loading with three free parameters, i.e. α, β and the ratio ε. If two coordinate axes are normalized to the crack length *a*, the gradient parameters can be treated as dimensionless

parameters. The computational strategy and solutions are valid for any gradient parameters of FGMs.

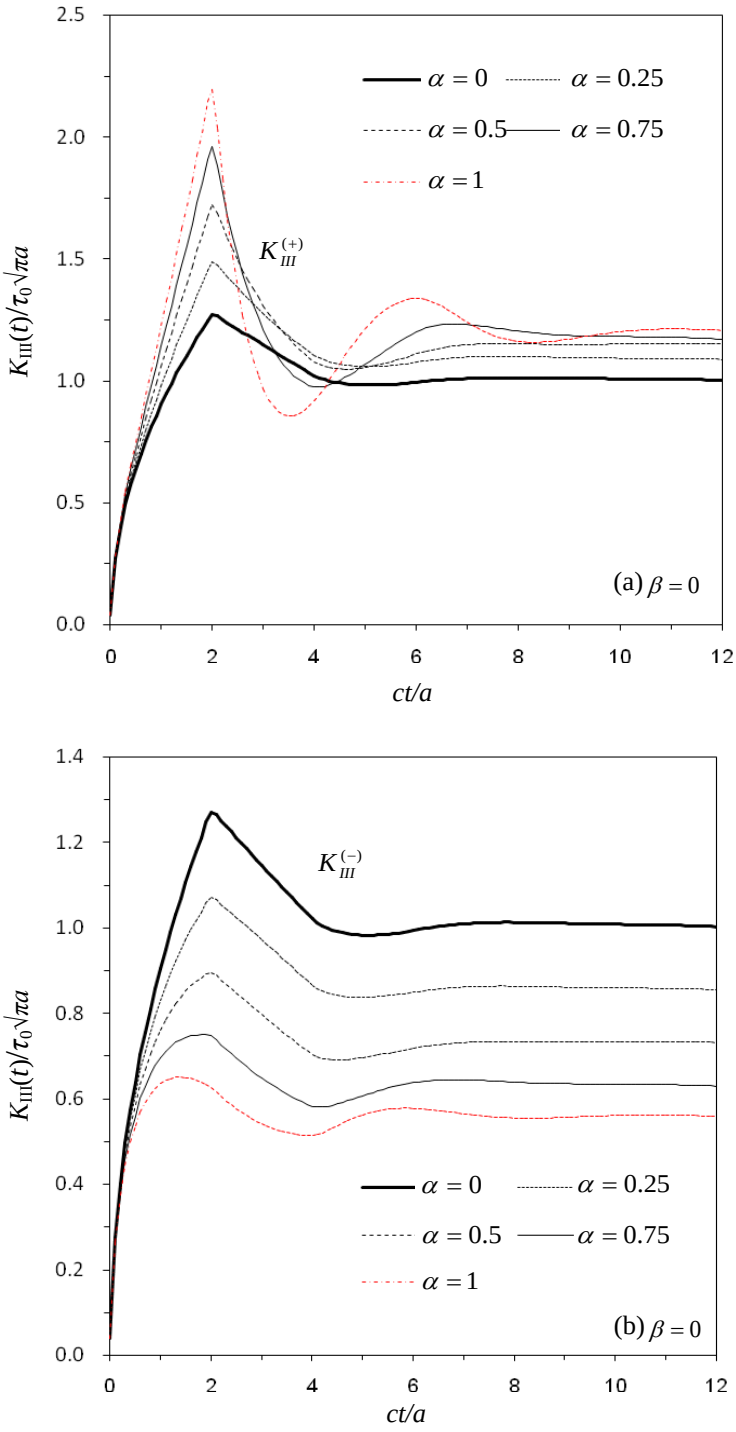

Figure 6, Normalized dynammic stress intensity factors of Case 1: (a) right crack-tip; (b) left crack-tip.

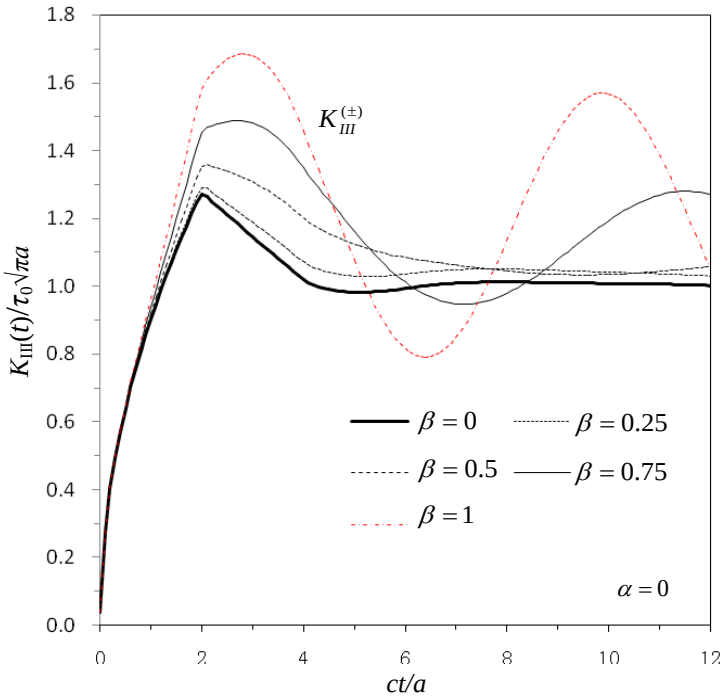

Figure 7, Normalized dynammic stress intensity factors of Case 2.

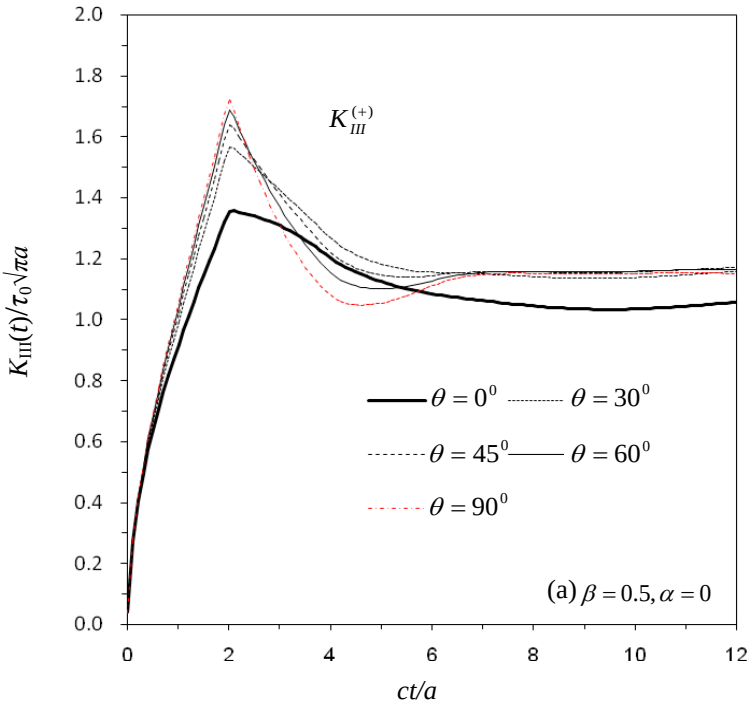

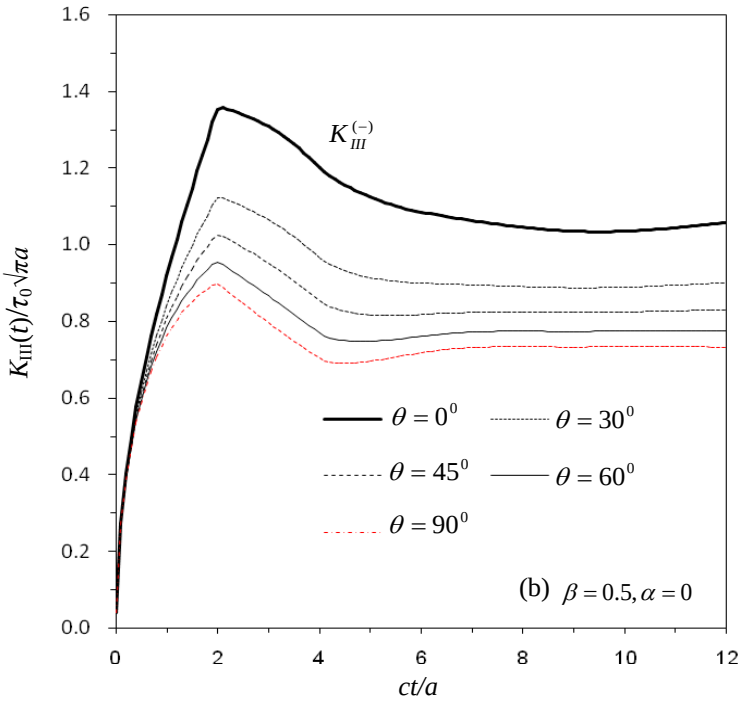

Figure 8. Normalized dynammic stress intensity factors of Case 3: (a) right crack-tip; (b) left crack-tip.

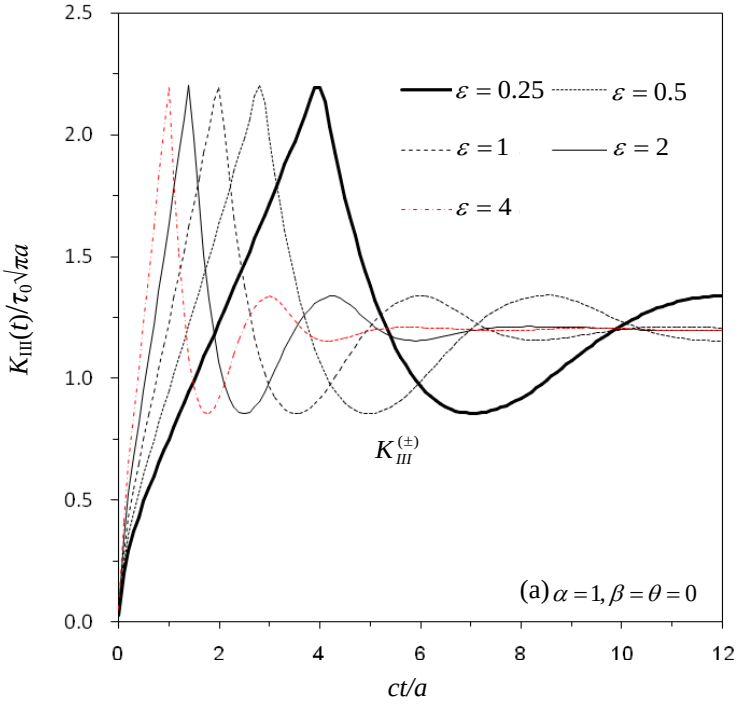

.

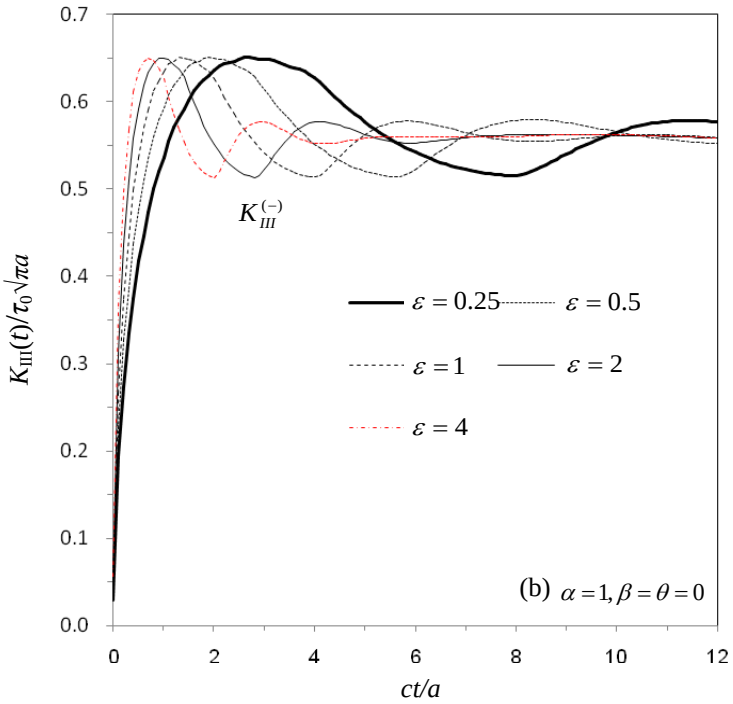

Figure 9. Normalized dynammic stress intensity factors of Case 4: (a) right crack-tip; (b) left crack-tip.

5. Conclusion

The fundamental solutions with anti-plane concentrated force and dislocation were derived in this paper for orthotropic FGMs. The influences of the material properties on the time- dependent shear stresses with a concentrated shear force were observed. For larger gradient parameters, oscillations occur for the shear stresses. For the application of these fundamental solutions, the first kind Fredholm integral equation was formulated for fracture problems with the Chebyshev series to determine the stress intensity factor for both static and dynamic loads. Dynamic anti-plane fracture problems were studied in the Laplace transformed domain and the Durbin's inverse transform method was employed. The static and the dynamic stress intensity factors were presented for different material parameters.

Acknowledgement

The first author would like to thank the support partially from the Natural and Science Foundation Council of China (No.11301040) and the Science Research Fund of Hunan Provincial Education Department (No.17B003). The second author like to thank the support partially from the National Natural Science Foundation of China (No.51608055).

References

1. Suresh S and Mortensen A. Fundamentals of Functionally Graded Materials, Institute of Materials, London, 1998.
2. Brebbia CA. The boundary element method for engineers. London/New York: Pentech Press/Halstead Press, 1978.
3. Aliabadi MH. Boundary element formulations in fracture mechanics. *Appl. Mech. Rev*. 1997; 50: 83-96.
4. Aliabadi MH. The boundary element method-applications in solids and structures. Chichester, Wiley, 2002.
5. Chen JT and Hong HK. Review of dual boundary element methods with emphasis on hypersingular integrals and divergent series. *Appl. Mech. Rev*. 1999;52: 17-33.
6. Cheng Alexander HD and Cheng Daisy T. Heritage and early history of the boundary element method. *Engng Analy. with Bound. Ele*. 2005;29: 268-302.
7. Clements DL and Budhi WS. A boundary element method for the solution of a class of steady-state problems. *Journal of Heat Transfer* 1999;121: 462-465.
8. Burgess G and Mahajerin A. A comparison of the boundary element method and superposition methods. *Comput. & Struct*. 1984;19:697-705.
9. Wen PH. Point intensity method of solving circular plate resting on elastical subgrade. *Eng. Mech.* 1987;4(2):18-26.
10. Wen PH. The numerical method for complex restrained problem of rectangular plate on elastic base. *J. Cen. South Inst. Min. Metall*. 1988;19(3):346-348.
11. Fairweather G and Karageorghis A. The method of fundamental solutions for elliptic boundary value problems. *Advances in Computational Mathematics* 1998;9:69-95.

12. Golberg MA and Chen CS. The method of fundamental solutions for potential, Helmholtz and diffusion problems. In: Golberg, M.A. (Ed.), Boundary Integral Methods: Numerical and Mathematical Aspects. Computational Mechanics Publications, Southampton, 1999.
13. Marin L and Lesnic D. The method of fundamental solutions for nonlinear functionally graded materials. *Int. J. Solids Struct*. 2007;44:6878-6890.
14. Crouch SL. Solution of plane elasticity problems by the displacement discontinuity method. Int *J Numer Meth Eng* 1976;10:301-43.
15. Crouch SL and Starfield AM. Boundary element methods in solid mechanics. London, George Allen & Unwin, 1983.
16. Dong CY and Pater CJ. Numerical implementation of displacement discontinuity method and its application in hydraulic fracturing. *Comput. Methods Appl. Mech. Eng.* 2002;191:745-60.
17. Liu Y. On the displacement discontinuity method and the boundary element method for solving 3-D crack problems. *Engng Fract. Mech*. 2016;164:35-45.
18. Shi J, Shen B, Stephansson O and Rinne M. A three-dimensional crack growth simulator with displacement discontinuity method. *Eng. Anal. Bound. Elem*. 2014;48:73-86.
19. Wen PH. Dynamic Fracture Mechanics: Displacement Discontinuity Method. Computational Mechanics Publications, Southampton UK and Boston USA, 1996.
20. Jin ZH and Batra RC. Some basic fracture mechanics concepts in functionally graded materials. *J. Mech. Phys. Solids* 1996;44:1221-1235.
21. Jin ZH and Batra RC. Interfacial cracking between functionally graded coatings and a substrate under antiplane shear. *Int. J. Engng Sci*. 1996;34 (15):1705-1716.
22. Nakagaki, M., Sasaki, H., Hagihara S.: A study of crack in functionally graded material under dyna- mic loading. Dynamic fracture failure and deformation. ASME PVP 300, 1-6 (1995).
23. Parameswaran, V., Shukla, A.: Dynamic fracture of a functionally gradient material having discrete property variation. J. Mater. Sci. 33, 3303- 3311 (1998).
24. Wang, B. L., Han, J. C., Du, S. Y.: Dynamic fracture mechanics analysis for composite materials with material inhomogeneity in thickness direction. Acta Mech. Solida Sinica 11, 84-93 (1998).
25. Babaei, R., Lukasiewicz, S. A.: Dynamic response of a crack in a functionally graded material between two dissimilar half planes under antiplane shear impact load. Engng. Fract. Mech. 60, 479-487 (1998).

26. Li C and Zou Z. Torsional impact response of a functionally graded material with a penny-shaped crack. *ASME J. Appl. Mech*. 1999;62:566-567.
27. Li C, Weng GJ, Duan Z, Zou Z. Dynamic stress intensity factor of a functionally graded material under antiplane shear loading. *Acta Mechanica* 2001; 149: 1-10.
28. Li C, Zhou Z, Duan Z. Dynamic stress field around the mode III crack tip in an orthotropic functionally graded material. *Applied Mathematics and Mechanics* (English Ed) 2000; 21(6): 651-658.
29. Choi HJ. Elastodynamic analysis of a crack at an arbitrary angle to the graded interfacial zone in bonded half-planes under antiplane shear impact. *Mech. Res. Commun*. 2006;33(5):636-650.
30. Zhang Ch, Savaidis A, Savaidis G and Zhu H. Transient dynamic analysis of a cracked functionally graded material by a BIEM. *Comput. Mater. Sci.* 2003;26:167-174.
31. Zhang Ch, Sladek J and Sladek V. Effects of material gradients on transient dynamc mode-III stress intensity factors in a FGM. *Int. J. Solids and Struct*. 2003;40:5251-5270.
32. Bateman H. Table of Integral Transforms, Vol. I, McGraw-Hill Book Company Inc, 1954.
33. Kaya MK and Erdogan F. On the solution of integral equations with strong singular kernels. *Q. Appl. Math.* 1987;45:105-122.
34. Durbin F. Numerical inversion of Laplace transforms: an efficient improvement to Dubner and Abate's method. *Comput. J*. 1974;17(4):371-376.
35. Koizumi M, Niino M.. Overview of FGM Research in Japan. *MRS Bulletin* 1995; 1: 19-21.
36. Cannillo V, Manfredini T, Montorsi M, Siligardi C, Sola A. Glass-alumina Functionally Graded Materials: their preparation and compositional profile evaluation. *Journal of the European Ceramic Society* 2006; 26(13): 2685-2693.